Title: Observation of incipient particle formation during flame synthesis by tandem differential mobility analysis-mass spectrometry (DMA-MS)

Authors: Yang Wang, Juha Kangasluoma, Michel Attoui, Jiaxi Fang, Heikki Junninen, Markku Kulmala, Tuukka Petäjä, and Pratim Biswas*

Abstract

While flame aerosol reactor (FLAR) synthesis of nanoparticles is widely used to produce a range of nanomaterials, incipient particle formation by nucleation and vapor condensation is not well understood. This gap in our knowledge of incipient particle formation is caused by limitations in instruments, where, during measurements, the high diffusivity of sub 3 nm particles significantly affects resolution and transport loss. This work used a high resolution Differential Mobility Analyzer (DMA) and an Atmospheric Pressure Interface-Mass Spectrometer (APi-TOF) to observe incipient particle formation during flame synthesis. By tandemly applying these two instruments, Differential Mobility Analysis-Mass Spectrometry (DMA-MS) measured the size and mass of the incipient particles simultaneously, and the effective density of the sub 3 nm particles was estimated. The APi-TOF further provided the chemical compositions of the detected particles based on highly accurate masses and isotope distributions. This study investigated the incipient particle formation in flames with and without the addition of synthesis precursors. Results from FLAR using two types of precursors including tetraethyl orthosilicate (TEOS) and titanium isopropoxide (TTIP) are presented. The effect of the precursor feed rates on incipient particle growth was also investigated.

Keywords: flame aerosol reactor (FLAR), combustion synthesis, incipient particle, differential mobility analysis (DMA), mass spectrometry (MS)

1. Introduction

Flame synthesis is a gas-phase approach for producing nanomaterials on an industrial scale, due to its high reaction temperature and fast reaction rates [1]. Flame-synthesized products, such as metal oxides and carbon-based materials, have been widely applied in catalysis [2], solar energy utilization [3], sensor technology [4], the rubber industry [5], and so on. During flame synthesis, the pyrolysis and oxidation of synthesis precursors, the clustering of vapor molecules, particle nucleation, and particle growth through coagulation, vapor condensation, and sintering, all take place in a single-step manner, resulting in a high yield of nanoparticles [6, 7]. The high temperature and fast reaction rate in flames, on the other hand, make it difficult to analyze detailed particle formation pathways. As the starting of the entire particle formation process, especially below 3 nm, significantly affect the characteristics of the final products, such as size, morphology, crystallinity, and chemical composition. However, research on the early stages of particle formation mechanisms is limited by the performance of existing instruments [8, 9]. The *in situ* measurement of particle size distributions in aerosol reactors commonly rely on Differential Mobility Analyzers (DMAs), which can classify a steady and narrowly monomobile stream of charged particles from particles with a continuous spectrum of electrical mobilities [10]. However, the high diffusivity of the sub 3 nm particles greatly decreases the resolution of conventional DMAs and increases the diffusion loss of the measured particles [11]. Molecular Beam Mass Spectrometry (MBMS) is typically used to analyze the composition of flame-generated particles, but the required low-pressure and fuel-rich environment often deviates from the actual operating conditions of flame synthesis [12]. These limitations pose difficulties in measuring incipient particles during flame synthesis, hindering a comprehensive understanding of the particle formation mechanisms.

With the development of a new set of instruments for investigating atmospheric particle nucleation [13] and for analyzing protein properties [14] in the past decade, measuring sub 3 nm particle size and mass

at atmospheric conditions has become feasible. DMAs with sheath flow rates of over 100 lpm are used to significantly reduce the residence time and the Brownian diffusion of particles in the instruments, increasing the resolution by orders of magnitude when measuring sub 3 nm particles [15]. The recently developed Atmospheric Pressure Interface Time-Of-Flight Mass Spectrometer (APi-TOF) is able to detect and analyze the chemical composition of atmospheric ions and charged clusters with high transmission and resolution [16]. Selected groups of molecular species were identified as playing an important role in atmospheric particle nucleation and growth [17]. Tandem Differential Mobility Analysis-Mass Spectrometry (DMA-MS) can simultaneously measure particle size and mass, and critical information on particle structure, charging characteristics, and formation mechanisms is obtained [18-20].

In this study, the incipient particle formation and growth below 3 nm in a premixed flat flame was investigated with the DMA-MS technique, where a high resolution DMA and an APi-TOF were used to counteract the particle Brownian diffusion and loss in the system. Direct measurement with the high resolution DMA coupled with an aerosol electrometer was conducted to provide the size distributions of particles generated during flame synthesis. The APi-TOF was used to determine the compositions of important intermediate particles during the synthesis of SiO_2 and TiO_2. The structure of the incipient flame-synthesized particles was further analyzed with the size and mass data measured by the DMA-MS.

2. Methods

2.1 Experimental Setup

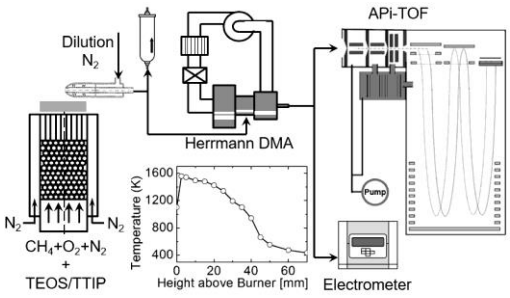

Figure 1. Schematic diagram of the experimental setup for measuring the incipient particles generated during flame synthesis. The Herrmann DMA classified particles with the same electrical mobility. The APi-TOF and the electrometer provided the mass spectrum and the concentration of the classified particles. The inset figure shows the temperature profile along the centerline above the burner.

Figure 1 shows the schematic diagram of the experimental setup. The system consisted a premixed flat flame burner, a dilution sampling probe, a high resolution DMA (Herrmann-type [21]), an APi-TOF (TOFWERK AG), and an aerosol electrometer (Model 3068B, TSI Inc.). A premixed flat flame was used in this study due to its uniformity and stability [22]. The stainless steel burner consisted of two concentric tubes with diameters of 0.75 inch and 1 inch, respectively, leaving a gap for passing a stream of N_2 (>99.95%, Linde AG) to protect the flame from the environment. In order to achieve a uniform velocity profile, the head of the burner was capped with a stainless steel honeycomb featuring a mesh size of 0.5 mm. Below the honeycomb cap, the inner tube was filled with 2 mm stainless steel beads for laminarizing the premixed flow streams. The gas mixture was composed of CH_4 (> 99.5%, Linde AG), O_2 (> 99.95%, Linde AG), and N_2, maintained at total flow rates of 1 lpm, 2.85 lpm, and 8 lpm respectively, with the help of mass flow controllers (MKS Inc.). The flame equivalence ratio (ϕ) was calculated to be 0.7. Organometallic precursors for synthesizing nanoparticles were introduced into the flame by bubbling a clean stream of N_2 though liquid precursors of tetraethyl orthosilicate (TEOS, >

98 %, Sigma-Aldrich Inc.) or titanium isopropoxide (TTIP, > 97 %, Sigma-Aldrich Inc.), at a temperature of 20 ^{o}C. At high temperatures in flames, these synthesis precursors reacted through thermal decomposition and oxidation to generate SiO_2 or TiO_2 nanoparticles, and previous studies demonstrated that a large amount of sub 3 nm particle were formed during these processes [8, 9, 11]. The feed rates of synthesis precursors were calculated according to the materials' saturation pressure data presented by Jang [23] for TEOS and Siefering and Griffin [24] for TTIP. Flame temperature was measured with a type R thermocouple, and the temperature profile is shown as the inset in Figure 1. Due to the low concentration of the synthesis precursors (as shown in Table 1), the effect of adding precursors on flame equivalence ratio and flame temperature were minimal. 5 mm above the head of the burner, a dilution sampling probe was used to introduce the flame-generated particles to downstream instruments while quenching further reactions and particle growth. By considering the thermal expansion of the sampled flow, a dilution ratio of 200 was attained [9]. Note that ionization sources were not applied in the system, implying that the downstream instruments measured the natively charged flame synthesized particles only. Due to a series of reported chemical ionization reactions, the flame acted as a neutral plasma that generated high concentrations of ions, which were sufficient to charge the incipient particles in the flame at various equivalence ratios [12]. It should be also noticed that not all of the flame-generated particles were charged, and the fraction of charged particles was a function of sampling height and flame conditions. To study the properties of neutral particles, well-characterized chemical ionization sources are needed to provide the neutral particles with known charges so that they can be detected by the instruments [25].

A Herrmann-type DMA was used to classify sub 3 nm particles with high resolution. The DMA was operated in a closed loop to maintain the same flow rate of the aerosol inlet and outlet flows. An inline blower (DOMEL Inc.) provided the recirculating sheath flow (> 500 lpm), and an inline filter and heat

exchanger removed the remaining particles and released the heat generated by the blower, respectively. The DMA classifies particles according to the relationship between the drag force and the electrostatic force. When a voltage (V) is applied across the electrodes of the DMA, the classified particles have a uniform mobility (Z) [10], which is further related to the size of a particle by $Z = Cne/3\pi\mu D_p$, where C is the Cunningham slip correction factor, n is the number of charges on the particle, e is the electronic charge, μ is the air viscosity, and D_p is the particle mobility size. For sub 3 nm particles, it is safe to assume that classified particles carry a single charge [26], which was also observed by the mass spectrometer during the experiments, since the isotope peaks that differ by mass units other than 1 were not detected. The potential across the DMA was applied by a high voltage source (Spellman Inc.) controlled by a Labview program. During the measurements, a step voltage of 3 V, a step time of 1 s, and a voltage scanning range of 100 to 1000 V were used to classify particles with size from 0.5 to 2 nm. It should be noted that the mobility size does not necessarily represent the particle physical size, especially for sub 3 nm particles whose chemical composition may significantly determine the structure of the cluster, while the size of non-spherical particles is poorly defined. Existing studies show that the particle mobility size subtracted by 0.3 nm agrees well with the volume size of the sub 3 nm clusters [18]. However, for simplicity, this study used particle mobility size as the indicator of particle physical size. At the same time, the inverse mobility values are marked in the graphs for reference. Before measuring the flame-generated particles, the DMA was first calibrated with the particles generated by electro-spraying a 0.2 mM tetraheptylammonium bromide-methanol solution [15]. The mobility of particles classified at an arbitrary DMA voltage can be accurately determined. We should also note that, although the DMA sheath flow is significantly increased, the high diffusivity of the sub 3 nm particles can still play a role in lowering the resolution of the DMA measurements, which is discussed in more detail in our previous work [11].

Downstream of the DMA, an aerosol electrometer (EM) collected the classified monomobile particles at a flow rate of 10 lpm. The recorded current was directly proportional to the charged particle concentration if particles carried one unit charge. In the following, the particle size distributions were qualitatively shown with the EM current as a function of particle size, since the data inversion of sub 3 nm particle size distributions was difficult to conduct due to the chemistry-dependent charging process [11]. The APi-TOF measured the mass-to-charge ratio (m/z) of the DMA-classified sub 3 nm particles. It can achieve a mass resolving power of 3000 Th/Th and a mass accuracy of 0.002%. The chemical composition of the measured particles was further analyzed by tofTools (a Matlab based set of programs [16, 27]), with the help of the highly accurate atomic mass and isotope distributions. Before measurements, the APi-TOF was calibrated with nitrate ions produced by a chemical ionization source. The DMA-MS technique simultaneously measures the particle size and the mass spectrum of the DMA-classified particles. The mass-size relationship further reveals the structure and effective density of the detected particles. This study investigated the mass-size relationship of the negatively charged particles only, since the positively charged particles were found to be unstable when they were transported from the DMA to the APi-TOF [20, 25, 28]. The obtained data are conveniently represented as contour plots, with the x-axis being the particle size or electrical mobility, and y-axis being m/z. The color of the data point denotes the relative abundance of the signal (black stands for the most intense signal, and white stands for the least intense signal).

2.2 Experimental Plan

Five sets of experiments were conducted in this study and tabulated in Table 1. Test 1 studied the properties of charged particles generated from blank flames without the addition of the precursors. Tests 2 and 3 were conducted with the addition of different types of precursors to investigate the formation

pathways of different types of nanoparticles. Tests 4 and 5, together with Test 2, further examined the influence of synthesis precursor feed rates on the incipient particle formation during flame synthesis.

Table 1. Experimental plan.

Test	Precursor Type	Feed rates [mmol/hr]
1	N/A	N/A
2	TEOS	0.118
3	TTIP	0.157
4	TEOS	0.235
5	TEOS	0.353

3. Results and Discussion

3.1 Particle formation in blank flames

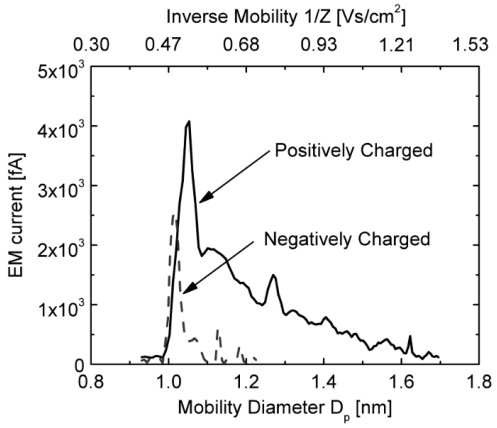

Figure 2. Size distributions of sub 3 nm particles generated from the blank flame.

Figure 2 shows the DMA-measured size distributions of the natively charged particles generated from the blank flame without the addition of the precursors. Charged particles below 1.8 nm in both polarities were observed in large quantities. The chemical ionization reactions in the flame are major sources of these charged particles [12]. The positively charged particles had a larger and broader distribution of sizes, yielding a relatively smaller electrical mobility compared to negatively charged particles. Similar results were observed in commonly used ionization sources such as radioactive neutralizers [20, 29] and corona dischargers [28]. The explanation for this phenomenon may be that, during the ionization process, the relatively large organic molecules act as positive charge carriers, while negative charge carriers are dominated by electrons. The electrons further combine with other molecules to form relatively smaller negatively charged particles with low proton affinities. Based on charge neutrality, the concentration difference between the positively and the negatively charged particles (Fig. 2) also indicated that the remaining negative charge carriers were electrons, whose electrical mobility is too high (> 1000 cm^2/Vs [12]) to be measured by the DMA. These charged particles may actively collide with nanoparticles during flame synthesis conditions. According to Fuchs charging theory [25], this

difference in the averaged electrical mobility will cause a higher fraction of particles carrying negative charges, which has been observed in previous studies [30, 31].

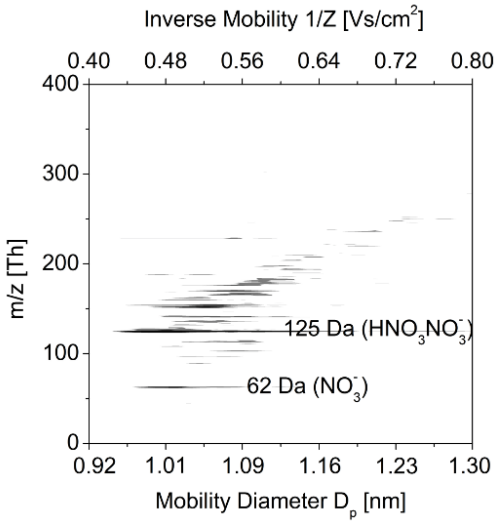

Figure 3. Contour plot showing the abundance of the blank flame-generated negatively charged particles as a function of size and m/z.

Figure 3 displays the mass-size relationship of the negatively charged particles generated from the blank flame. At the inverse mobility of 0.48 Vs/cm^2 (mobility size of 1.01 nm) where the EM detected the highest particle concentration (Fig. 2), the mass spectrum indicated that these particles were mainly composed of nitrate ions (NO_3^- at m/z of 62 Th, and $HNO_3 \cdot NO_3^-$ at m/z of 125 Th). The formation of these nitrate ions might be caused by the active NO_x production in the blank flame, especially when the combustible mixture was premixed and the flame was operated in a fuel-lean condition [32]. The NO_x species may further react with water vapor to form nitrate ions. Due to their low proton affinities, these nitrate ions became the dominant negative charge carriers, which was also observed in other types of ionization sources [20, 28, 33]. The existence of two different masses (62 Da and 125 Da) corresponding to a same mobility size (1.01 nm) suggested that the ions might be fragmented when they transported from the DMA to the APi-TOF. Aside from the nitrate ions, negatively charged particles with sizes and

masses larger than 1.01 nm and 125 Da respectively were also detected. They were probably generated during the collision between electrons with relatively larger organic molecules. The detection of a spectrum of ions implied the complexity of chemical ionization reactions and the following particle charging process in flames.

3.2 Addition of flame synthesis precursors

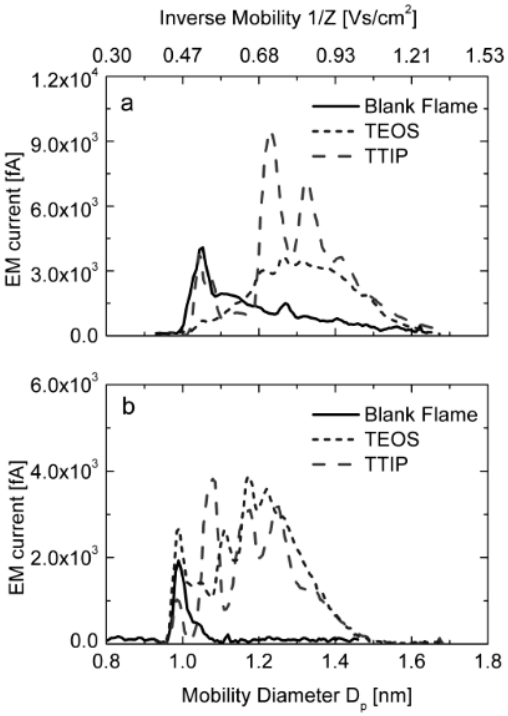

Figure 4. Size distributions of sub 3 nm charged particles under different synthesis conditions. a) positively charged particles; b) negatively charged particles. Note different scales of y-axes.

The sub 3 nm particle size distributions obtained under different synthesis conditions are shown in Fig. 4. When synthesis precursors were added to the flame, the DMA measurements detected particles larger than flame-generated particles, as a result of particle formation and growth. The sizes of these particles were also found to be discrete instead of continuous, which implied that certain stable species might act as important intermediates during particle formation. The average size and concentration of the

219 positively charged particles was still greater than those of the negatively charged particles, where the
220 existence of relatively small charge carriers might play an important role, as explained above.
221

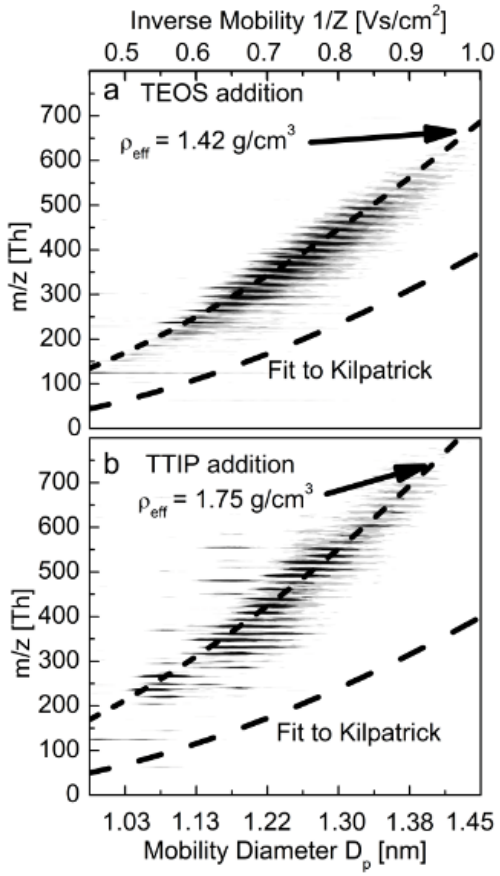

222

223 **Figure 5**. Contour plots showing the abundance of negatively charged particles during flame synthesis
224 conditions as a function of size and m/z. a) using TEOS as synthesis precursor with a feed rate of 0.118
225 mmol/hr; b) using TTIP as synthesis precursor with a feed rate of 0.157 mmol/hr. The mass-size
226 relationships assuming that particles were spherical are displayed as short-dashed lines. The fit to
227 Kilpatrick's mass-mobility relationship is displayed as long-dashed lines.
228
229

Table 2. Chemical compositions of major negatively charged particles detected by the APi-TOF under different flame conditions.

Blank flame		TEOS addition		TTIP addition	
Chemical formula	**m/z**	**Chemical formula**	**m/z**	**Chemical formula**	**m/z**
NO_3^-	61.9878	NO_3^-	61.9878	NO_3^-	61.9878
$HNO_3 \cdot NO_3^-$	124.9835	$Si_2H_6NO_{10}^-$	235.9530	$TiN_2O_{10}^-$	235.9032
		$Si_3H_6NO_{12}^-$	295.9198	$TiN_3O_{11}^-$	265.9012
		$Si_3H_8NO_{13}^-$	313.9303	$Ti_2NO_{11}^-$	285.8437
		$Si_4H_{10}NO_{16}^-$	319.9077	$Ti_2N_2O_{14}^-$	347.8308

The mass-size relationships of the flame-generated sub 3 nm particles during synthesis conditions are shown in Fig. 5. Major negatively charged species, such as $Si_2O_4(H_2O)_3NO_3^-$ (236 Th), $Si_3O_6(H_2O)_3NO_3^-$ (296 Th), $TiO_2(NO_3)_3^-$ (266 Th), and $Ti_2O_8(NO_3)_2^-$ (348 Th) were detected by the APi-TOF. Table 2 lists the incipient particles with identified compositions and atomic masses. The existence of nitrate ions in the silicon and titanium-containing particles implied a strong interaction between the flame-generated ions and the synthesized particles. Since flame synthesis is conducted with N_2 as the diluting gas on many occasions, these detected ions may act as contaminants for particle growth and crystallization. Hence, further studies investigating the incipient particle formation mechanisms without N_2 participation are needed. Figure 5 also shows that the detected particles fell into different bands with strong signal intensities. A lot of these bands were separated by the atomic masses of N (14 Da), O (18 Da), or H_2O (18 Da), instead of by the atomic mass of SiO_2 (60 Da) or TiO_2 (80 Da). This result suggested the high involvement of blank flame-generated species in particle synthesis. To confirm that the measured charged particles represent the characteristics of those generated in the flame, further experiments using an enhanced condensation particle counter and a charged particle remover was conducted. Results show that under the tested conditions, the charging fraction of sub 3 nm

particles is extremely high, where more than 90% of the flame-generated sub 3 nm particles were charged [34]. The high charge fraction also contradicts the classical charging theories, suggesting that further studies on the charging mechanisms of particles in flames are needed.

Depending on the type of nanoparticles synthesized, the mass-size relationships show different trends in Fig. 5. At a same mobility size of 1.30 nm, the particles generated from TTIP reactions (~ 550 Da) were heavier than the particles generated from TEOS reactions (~ 420 Da), which was possibly caused by the higher atomic mass of titanium. Based on the mass and mobility size values, an effective density (ρ_{eff}) could be calculated for these incipient particles following the method introduced below. By assuming that the detected particles were spherical, the effective density satisfied the relationship of $m = \pi D_p^3 \rho_{eff} / 6$, where m is the particle mass and D_p is the particle size. The value of the effective density should guarantee that most of the data points in the contour plot fall on the curve representing the spherical particle mass-size relationship. Further calculation indicated that using particle volume size (mobility size subtracted by 0.3 nm [18]) as D_p provided a better fit when calculating ρ_{eff}, since the mobility size of a particle overestimates the physical size below 3 nm, due to the enhanced interaction between the charged cluster and the dipole it induced in the gas molecules [18]. The particles generated from flames with the addition of TEOS and TTIP had effective densities of 1.42 g/cm^3 and 1.75 g/cm^3, respectively. These incipient particles were less dense than the SiO_2 and TiO_2 bulk crystals (2.65 g/cm^3 and 4.23 g/cm^3), possibly because these particles were in an amorphous state, where the atoms were not tightly packed. The attachment of the species other than oxides, such as nitrate and organic molecules, on these incipient particles might also lower the density of the detected particles.

The simultaneously measured mobility and mass of the flame-generated incipient particles could be compared with the data calculated from empirically determined mass-mobility relationships. The most

widely used mass-mobility relationship was presented by Kilpatrick [35] and was further fitted with a function of

$$Z = \exp[-0.0347\ \ln^2(m) - 0.0376\ \ln(m) + 1.4662\,], \quad (1)$$

where Z and m represent the particle electrical mobility (unit: cm^2/Vs) and atomic mass (unit: Da), respectively [36]. The fitted functions of Kilpatrick's mass-mobility relationship are also displayed in Fig. 5, showing that, at a same electrical mobility, the actual particle mass is higher than the mass predicted by the empirical relationship. This discrepancy can be explained by the fact that the electrical mobility is largely determined by the structure of particles, while particles with similar structures can have different chemical compositions and atomic masses. Due to the existence of relatively heavy species such as silicon and titanium, the flame-generated incipient particles had higher masses. Since researchers often rely on Kilpatrick's relationship to convert the measured mobility to the mass of particles in order to decipher the particle composition, this measured result proves that the existing mass-mobility relationships will be dependent on the type of chemical species. Directly using these relationships may therefore cause errors. To better predict the mass-mobility relationships, numerical methods were used by researchers to consider the physical collision and potential interaction between the molecular clusters and particles, where a desirable agreement was observed between the calculated and the experimentally measured mass and mobility data [37].

3.3 Effect of the synthesis precursor feed rates

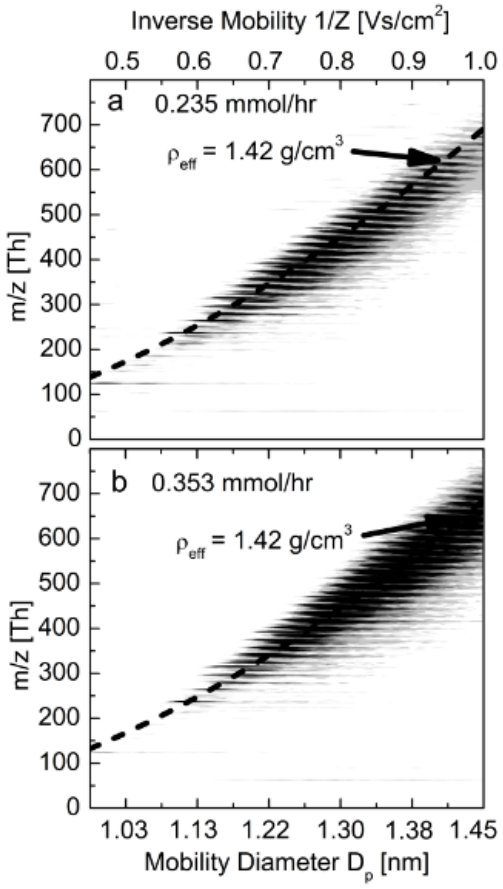

Figure 6. Contour plots showing the abundance of negatively charged particles generated at different TEOS feed rates as a function of size and m/z. a) TEOS feed rate of 0.235 mmol/hr; b) TEOS feed rate of 0.353 mmol/hr. The mass-size relationships assuming that particles were spherical are displayed as short-dashed lines.

Figure 6 shows the effect of TEOS feed rates on the DMA-MS measured incipient particle size and mass distributions. The concentration of the particles with larger sizes and masses increased as more precursors were fed to the flame, indicating a stronger particle growth process by vapor condensation and coagulation. The concentration of the smaller charged particles with low mass and size decreased due to coagulation and the scavenging effect caused by the existing larger particles. The calculated effective density remained the same (Fig. 6), demonstrating that the particle formation pathway did not change as a function of precursor feed rates.

4. Conclusions

The incipient particle formation during flame synthesis was investigated for the first time using the tandem DMA-MS technique. A high resolution DMA and an APi-TOF were used to measure the size and mass of the sub 3 nm particles simultaneously in the flames without the addition of synthesis precursors and with the addition of TEOS or TTIP.

Measurements in a blank flame detected a large number of sub 3 nm particles generated from chemical ionization reactions, and determined that nitrate ions dominated in the negative ions. The formation of nitrate ions may be related with the NO_x formation in flames. Measurements conducted with the addition of synthesis precursors found particles with discrete size distributions, indicating the existence of stable particles as important intermediates during flame synthesis. The blank flame-generated ions played an important role during particle synthesis, since the APi-TOF observed the appearance of nitrate ions in particles containing silicon or titanium. Future work on flame synthesis while manipulating the ion properties, may bring new perspectives on manufacturing functional nanomaterials at high temperatures. The effective densities of the incipient particles were calculated by assuming that the particles were spheres. These particles had lower densities than the bulk materials of SiO_2 and TiO_2, possibly because of the impurities in the particles and their amorphous structures. The commonly used Kilpatrick's mass-mobility relationship was also evaluated in this study, and the difference between the measured data and the Kilpatrick's relationship suggested that particle compositions largely determined particle mass and mobility. As precursor feed rate increased, particles with larger mass and sizes were formed due to enhanced coagulation and vapor condensation. The unchanged particle effective density implied that the particle formation pathway in flames was not a function of precursor feed rates.

Acknowledgements

This work is supported by the Solar Energy Research Institute for India and the United States (SERIIUS), funded jointly by the U.S. Department of Energy (Office of Science, Office of Basic Energy Sciences, and Energy Efficiency and Renewable Energy, Solar Energy Technology Program, under Subcontract DE-AC36-08GO28308 to the National Renewable Energy Laboratory, Golden, Colorado) and the Government of India, through the Department of Science and Technology under Subcontract IUSSTF/JCERDC-SERIIUS/2012. The work was also supported by Academy of Finland via Center of Excellence project in Atmospheric Sciences (272041) and European Commission via ACTRIS2 (654109).

References:

[1] P. Roth, Proc. Combust. Inst. 31 (2007) 1773-1788.
[2] F. Niu, S. Li, Y. Zong, Q. Yao, J. Phys. Chem. C, 118 (2014) 19165-19171.
[3] E. Thimsen, N. Rastgar, P. Biswas, J. Phys. Chem. C 112 (2008) 4134-4140.
[4] S. Bakrania, C. Perez, M. Wooldridge, Proc. Combust. Inst. 31 (2007) 1797-1804.
[5] P.T. Spicer, C. Artelt, S. Sanders, S.E. Pratsinis, J. Aerosol Sci. 29 (1998) 647-659.
[6] J. Jiang, D.-R. Chen, P. Biswas, Nanotechnology, 18 (2007) 285603.
[7] Y. Zhang, L. Shuiqing, S. Deng, Q. Yao, S.D. Tse, J. Aerosol Sci. 44 (2012) 71-82.
[8] J. Fang, Y. Wang, M. Attoui, T.S. Chadha, J.R. Ray, W.-N. Wang, Y.-S. Jun, P. Biswas, Anal. Chem. 86 (2014) 7523-7529.
[9] Y. Wang, P. Liu, J. Fang, W.-N. Wang, P. Biswas, J. Nanopart. Res. 17 (2015) 1-13.
[10] E. Knutson, K. Whitby, J. Aerosol Sci. 6 (1975) 443-451.
[11] Y. Wang, J. Fang, M. Attoui, T.S. Chadha, W.-N. Wang, P. Biswas, J. Aerosol Sci. 71 (2014) 52-64.
[12] A.B. Fialkov, Prog. Energy Combust. Sci. 23 (1997) 399-528.
[13] M. Kulmala, J. Kontkanen, H. Junninen, K. Lehtipalo, H.E. Manninen, T. Nieminen, T. Petäjä, M. Sipilä, S. Schobesberger, P. Rantala, Science 339 (2013) 943-946.
[14] C.J. Hogan Jr, J.F. de la Mora, J. Am. Soc. Mass. Spectrom. 22 (2011) 158-172.
[15] J. Fernandez de la Mora, Aerosol Measurement: Principles, Techniques, and Applications, John Wiley & Sons, Inc., Hoboken, New Jersey, U.S., 2011, p. 697.
[16] H. Junninen, M. Ehn, T. Petäjä, L. Luosujärvi, T. Kotiaho, R. Kostiainen, U. Rohner, M. Gonin, K. Fuhrer, M. Kulmala, Atmos. Meas. Tech. 3 (2010) 1039-1053.
[17] M. Ehn, J.A. Thornton, E. Kleist, M. Sipilä, H. Junninen, I. Pullinen, M. Springer, F. Rubach, R. Tillmann, B. Lee, Nature 506 (2014) 476-479.
[18] C. Larriba, C.J. Hogan Jr, M. Attoui, R. Borrajo, J.F. Garcia, J.F. de la Mora, Aerosol Sci. Technol. 45 (2011) 453-467.
[19] A. Maißer, V. Premnath, A. Ghosh, T.A. Nguyen, M. Attoui, C.J. Hogan, PCCP 13 (2011) 21630-21641.
[20] A. Maißer, J.M. Thomas, C. Larriba-Andaluz, S. He, C.J. Hogan, J. Aerosol Sci. 90 (2015) 36-50.
[21] W. Herrmann, T. Eichler, N. Bernardo, J. Fernández de la Mora, Annual Conference of the American Association for Aerosol Research, St. Louis, MO, U.S., 2000.
[22] X. Wang, E. Cotter, K.N. Iyer, J. Fang, B.J. Williams, P. Biswas, Proc. Combust. Inst. 35 (2015) 2347-2354.
[23] H.D. Jang, Aerosol Sci. Technol. 30 (1999) 477-488.
[24] K. Siefering, G. Griffin, J. Electrochem. Soc. 137 (1990) 1206-1208.
[25] J. Kangasluoma, M. Attoui, H. Junninen, K. Lehtipalo, A. Samodurov, F. Korhonen, N. Sarnela, A. Schmidt-Ott, D. Worsnop, M. Kulmala, J. Aerosol Sci. 87 (2015) 53-62.
[26] N. Fuchs, Geofis. pura appl. 56 (1963) 185-193.
[27] H. Junninen, *Data Cycle in Atmospheric Physics: from Detected Millivolts to Understanding the Atmosphere*, PhD thesis, University of Helsinki, Helsinki, Finland, 2014.
[28] H. Manninen, A. Franchin, S. Schobesberger, A. Hirsikko, J. Hakala, A. Skromulis, J. Kangasluoma, M. Ehn, H. Junninen, A. Mirme, Atmos. Meas. Tech. Discuss. 4 (2011) 2099-2125.
[29] P. Kallinger, G. Steiner, W.W. Szymanski, J. Nanopart. Res. 14 (2012) 1-8.
[30] M.M. Maricq, Aerosol Sci. Tech. 42 (2008) 247-254.
[31] M. Sahu, J. Park, P. Biswas, J. Nanopart. Res. 14 (2012) 1-11.
[32] S.R. Turns, An introduction to combustion, McGraw-Hill, New York, U.S., 1996.

[33] G. Steiner, T. Jokinen, H. Junninen, M. Sipilä, T. Petäjä, D. Worsnop, G.P. Reischl, M. Kulmala, Aerosol Sci. Technol. 48 (2014) 261-270.
[35] Y. Wang, J. Kangasluoma, M. Attoui, H. Junninen, M. Kulmala, T. Petäjä, P. Biswas, Anal. Chem. *Submitted*.
[35] W. Kilpatrick, in: Proc. Annu. Conf. Mass Spectrosc, 1971, pp. 320-325.
[36] J.M. Mäkelä, V. Jokinen, T. Mattila, A. Ukkonen, J. Keskinen, J. Aerosol Sci. 27 (1996) 175-190.
[37] C. Larriba, C.J. Hogan Jr, J. Phys. Chem. A, 117 (2013) 3887-3901.

Tables

Table 1. Experimental plan.

Test	Precursor Type	Feed rates [mmol/hr]
1	N/A	N/A
2	TEOS	0.118
3	TTIP	0.157
4	TEOS	0.235
5	TEOS	0.353

Table 2. Chemical compositions of major negatively charged particles detected by the APi-TOF under different flame conditions.

Blank flame		**TEOS addition**		**TTIP addition**	
Chemical formula	**m/z**	**Chemical formula**	**m/z**	**Chemical formula**	**m/z**
NO_3^-	61.9878	NO_3^-	61.9878	NO_3^-	61.9878
$HNO_3 \cdot NO_3^-$	124.9835	$Si_2H_6NO_{10}^-$	235.9530	$TiN_2O_{10}^-$	235.9032
		$Si_3H_6NO_{12}^-$	295.9198	$TiN_3O_{11}^-$	265.9012
		$Si_3H_8NO_{13}^-$	313.9303	$Ti_2NO_{11}^-$	285.8437
		$Si_4H_{10}NO_{16}^-$	319.9077	$Ti_2N_2O_{14}^-$	347.8308

List of Figure Captions

Figure 1. Schematic diagram of the experimental setup for measuring the incipient particles generated during flame synthesis. The Herrmann DMA classified particles with the same electrical mobility. The APi-TOF and the electrometer provided the mass spectrum and the concentration of the classified particles. The inset figure shows the temperature profile along the centerline above the burner.

Figure 2. Size distributions of sub 3 nm charged particles generated from the blank flame.

Figure 3. Contour plot showing the abundance of the blank flame-generated negatively charged particles as a function of size and m/z.

Figure 4. Size distributions of sub 3 nm charged particles under different synthesis conditions. a) positively charged particles; b) negatively charged particles. Note different scales of y-axes.

Figure 5. Contour plots showing the abundance of negatively charged particles during flame synthesis conditions as a function of size and m/z. a) using TEOS as synthesis precursor; b) using TTIP as synthesis precursor. The mass-size relationships assuming that particles were spherical are displayed as short-dashed lines. The fit to Kilpatrick's mass-mobility relationship is displayed as long-dashed lines.

Figure 6. Contour plots showing the abundance of negatively charged particles generated at different TEOS feed rates as a function of size and m/z. a) TEOS feed rate of 0.235 mmol/hr; b) TEOS feed rate of 0.353 mmol/hr. The mass-size relationships assuming that particles were spherical are displayed as short-dashed lines.